Profiles of Light-Induced Charge Gratings on Photorefractive Crystals

E. Soergel* and W. Krieger
Max-Planck-Institut für Quantenoptik, Hans-Kopfermann-Strasse 1, 85748 Garching, Germany
(Received 25 January 1999)

The profiles of light-induced charge gratings on photorefractive $Bi_{12}SiO_{20}$ crystals are directly observed by electrostatic force imaging with an atomic force microscope. We investigate the temporal evolution of the profiles during grating formation and the dependence of the profiles of saturated gratings on the fringe spacing and the modulation index of the light grating. In the case of saturated gratings, the profiles are well described by a simple theoretical model.

PACS numbers: 42.70.Nq, 42.65.Hw, 61.16.Ch

The photorefractive effect offers a wide range of applications, which are currently being extensively investigated [1]. It occurs in materials that are simultaneously photoconductive and electro-optic. In such materials a spatially modulated light field leads to a redistribution of charges, and the accompanying space-charge field gives rise to a refractive index pattern. In general, this pattern is not an exact replica of the light-intensity distribution. Its form develops, driven by a number of processes: the excitation of charge carriers by the incident light, charge transport by diffusion and drift, and the recapture of the carriers in traps. These processes are modeled in a set of coupled differential equations introduced by Kukhtarev [2]. A general solution of these equations in closed form is not available. The profiles of space-charge fields generated by an interference pattern of two laser beams have been calculated numerically [3] and, under special assumptions, also analytically [4].

It is surprising that there has hitherto been little experimental effort to directly determine the patterns stored in the photorefractive materials. Such investigations would be a powerful tool for exploring the dynamics of the photorefractive effect. In the few experiments previously reported, images of refractive-index gratings were obtained by optical techniques [5,6], charge gratings were detected with an electron microscope [7], and their profiles were probed with pressure waves [8]. The spatial resolution achieved in [8] was 15 μm, and in the case of optical mapping it is limited by the wavelength. The electron micrographs suffered from poor signal-to-noise ratio. A comparison with theoretical grating profiles was not attempted. Indirect experimental information about the profiles of refractive-index gratings can also be obtained by the measurement of higher-order Bragg diffraction [9]. These diffracted components have very small intensities, and therefore it is difficult to derive grating profiles from an addition of harmonic terms.

We used charge detection with an atomic force microscope (AFM) to directly image light-induced charge gratings on photorefractive $Bi_{12}SiO_{20}$ and $BaTiO_3$ crystals with a lateral resolution of a few 10 nm and a sensitivity that even allowed us to detect a charge nanostructure at the crystal surfaces [10,11]. This method is applied here to investigate the profiles of charge gratings on $Bi_{12}SiO_{20}$ crystals. For the first time, the development of the grating profile during grating buildup is directly observed, as well as the dependence of the profiles of saturated charge gratings on the fringe spacing and the modulation index of the light grating. The profiles of saturated gratings are well described by a simple theoretical model. Astonishingly, an electrostatic potential measurement was already used before the advent of the AFM to study charge distributions generated by a single laser beam in $LiNbO_3$, however, with a spatial resolution of only 0.1 mm [12].

Our homebuilt AFM is presented in detail elsewhere [10]. For charge detection it is operated in the noncontact mode. A schematic drawing of the photorefractive sample, the tip, and the cantilever is shown in Fig. 1(a). A sinusoidal voltage periodically charges the tip. The

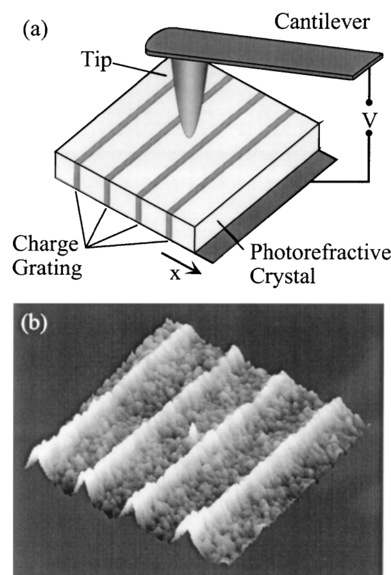

FIG. 1. (a) Schematic view of the setup for the detection of charge gratings on photorefractive crystals with the force microscope (V = sinusoidal voltage applied between tip and back electrode). (b) Charge grating detected on a $Bi_{12}SiO_{20}$ crystal. The charge signal is plotted versus the surface coordinates (fringe spacing 2.7 μm, image size 10 μm $\times$ 10 μm).

 0031-9007/99/83(12)/2336(4)$15.00 © 1999 The American Physical Society

electrostatic force between this periodic charge and the surface charge to be measured is detected with a lock-in amplifier [13]. This signal is proportional to the surface-charge density, and we therefore also refer to it as charge signal. The phase sensitivity of the measurement allows us to determine the polarity of the surface charges. The lateral resolution is determined by the macroscopic radius of curvature of the probing tip, typically 30 nm.

The $Bi_{12}SiO_{20}$ crystal samples ($5 \times 6 \times 1$ mm^3) [14] are attached to a 90° prism, and the charge gratings are generated by two interfering argon-ion laser beams ($\lambda = 514$ nm) in a total-internal-reflection geometry as shown in Fig. 2. The orientation of the grating planes is perpendicular to the surface. The fringe spacing is varied by choosing different angles between the incident beams. To change the modulation index, we attenuate one of the laser beams with neutral density filters.

For image acquisition, the crystal is scanned beneath the tip. Stored charge gratings are therefore imaged, with the writing beams switched off. Such a grating is shown in Fig. 1(b). The charge signal is plotted in a three-dimensional view. The image size is 10 μm $\times$ 10 μm. Before image acquisition was started, the crystal was illuminated for 1 s with two laser beams of 100 mW/cm^2 each. Four bright, negatively charged grating lines with a fringe spacing of 2.7 μm are clearly visible. The scan starts at the lower left of the figure. During the acquisition time of 70 min, a slight decay of the grating amplitude is observed. At the end of the image, the amplitude corresponds to an electrostatic force of 15 pN between the tip and sample. The granular substructure of the charge signal is not caused by the noise of the detection system. We attribute this structure to crystal imperfections and the effects of surface polishing [10,11]. The grating profiles presented in this Letter were obtained by averaging over parts of charge images as in Fig. 1(b), thereby eliminating the crystal inhomogeneities. In order to exclude possible effects of the grating decay on the grating profile, the acquisition time was limited to 5 min.

In a first experiment we observed the temporal evolution of such charge-grating profiles during the writing process. Profiles obtained for different exposure times are presented in Fig. 3. The intensity of the writing beams was 1.35 mW/cm^2 each, and the fringe spacing was 2.7 μm. Both the amplitude and the shape of the grating profile are observed to change considerably during grating formation: the amplitude increases by a factor of 6, whereas the width decreases by a factor of 2. The charge grating reproduces the sinusoidal shape of the light grating only with the shortest exposure times. With longer times we observe the buildup of narrow, negatively charged lines. From simultaneous measurements of the light intensity and charge distribution [11] we know that these lines correspond to the dark grating positions. In the $Bi_{12}SiO_{20}$ crystal the photoexcited charge carriers accumulating at the dark positions are therefore predominantly electrons.

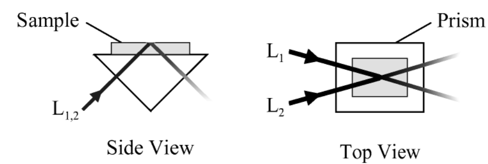

FIG. 2. Optical setup for the generation of charge gratings in a photorefractive sample (L_1, L_2 = laser beams).

The buildup of narrow lines at the dark positions shows the integrating nature of the photorefractive effect. The width of these lines is related to the diffusion length of the charge carriers in the crystal [3]. With exposure times longer than 10 s the grating profile was observed to remain unchanged; it is then said to be saturated.

We also observed the dark decay of saturated charge gratings with fringe spacings of 2.7 and 10 μm. The decrease of the grating amplitude could be described by a double exponential decay ($t_1 = 23$ min and $t_2 = 450$ min), but the shape of profiles showed no change at all [15].

In further experiments we determined the dependence of the profiles of saturated gratings on the fringe spacing Λ and on the modulation index m of the light grating. Charge-grating profiles for $m = 1$ and different fringe spacings are presented in Fig. 4. The grating amplitudes are normalized to the same value. A drastic change of the grating profile from nearly sinusoidal (for $\Lambda = 0.25$ μm) to extremely anharmonic (for $\Lambda = 4$ μm) is clearly observed. For $\Lambda \geq 1.6$ μm the width of the maxima remains approximately constant (≈ 0.5 μm).

Figure 5 shows the dependence of saturated charge-grating profiles on the modulation index of the light

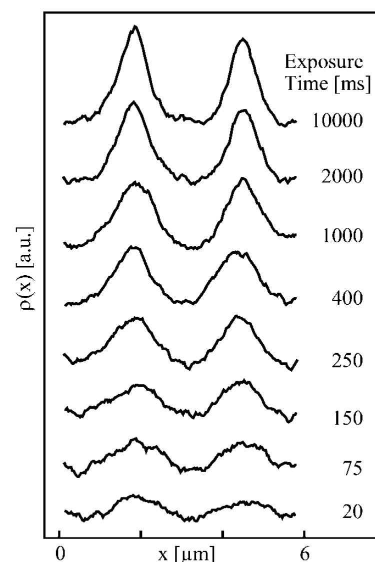

FIG. 3. Temporal evolution of the charge grating profile on a $Bi_{12}SiO_{20}$ crystal during the writing process obtained by varying the exposure time [fringe spacing 2.7 μm, laser intensity 1.35 mW/cm^2, $\rho(x)$ = charge signal, x = position].

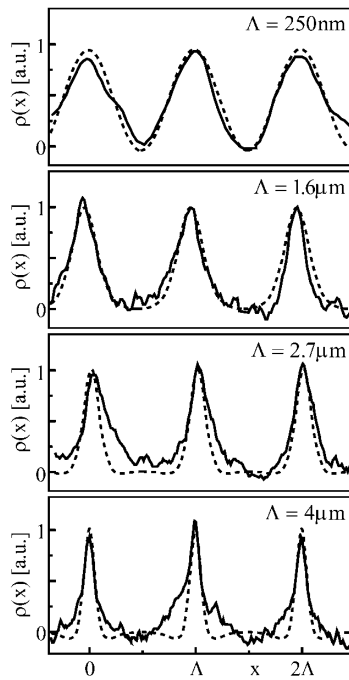

FIG. 4. Charge grating profiles on a $Bi_{12}SiO_{20}$ crystal with different fringe spacings Λ, modulation index $m = 1$. The dotted curves are theoretical fits as described in the text. The grating amplitudes are normalized to the same height [$\rho(x) =$ charge signal, $x =$ position].

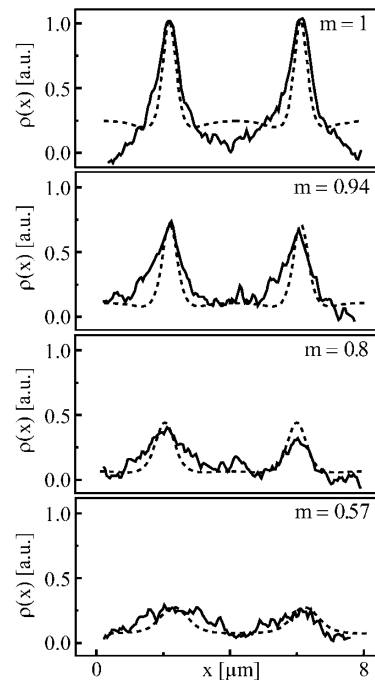

FIG. 5. Charge grating profiles on a $Bi_{12}SiO_{20}$ crystal obtained with different modulation indices m of the laser field (fringe spacing 4 μm). The dotted curves are theoretical fits as described in the text [$\rho(x) =$ charge signal, $x =$ position].

grating at a fringe spacing of 4 μm. The intensity of the stronger beam was 35 mW/cm^2 and the writing time was 5 s. As the modulation index grows, the lines of negative charge are seen to increase in amplitude and decrease in width.

Saturated grating profiles of the space charge field in photorefractive materials have already been calculated in a very early paper by Amodei [16]. The interference pattern of two laser beams with intensities I_1 and I_2 is given by

$$I(x) = I_0(1 + m\cos Kx), \tag{1}$$

where $I_0 = I_1 + I_2$, the modulation index $m = 2\sqrt{I_1 I_2}/(I_1 + I_2)$, and $K = 2\pi/\Lambda$. Amodei then assumes the density of photoexcited charge carriers $n(x)$ to be a replica of the intensity distribution (1) throughout the writing process, i.e., $n(x) = n_0(1 + m\cos Kx)$. The spatial variation of $n(x)$ gives rise to a diffusion current $j_{\mathrm{diff}} = \mu k_B T[\partial n(x)/\partial x]$, with μ representing the free-carrier mobility, k_B the Boltzmann constant, and T the temperature. The resulting redistribution of charges leads to the buildup of a space-charge field $E_{\mathrm{sc}}(x)$, which in turn generates a drift current $j_{\mathrm{drift}} = q\mu n(x)E_{\mathrm{sc}}(x)$, with q the elementary charge. Under steady-state conditions the current density is zero everywhere in space, i.e., $j_{\mathrm{diff}} + j_{\mathrm{drift}} = 0$. From this condition the space-charge field is obtained as

$$E_{\mathrm{sc}}(x) = \frac{mk_BTK}{q}\,\frac{\sin Kx}{1 + m\cos Kx}. \tag{2}$$

This expression diverges for $m \rightarrow 1$ at the dark grating lines ($Kx = \pi$), since the model does not take into account that the number of traps in the crystal is limited and that the free charge carriers have a finite diffusion length. To account for the latter, we assume a washed-out distribution of free charge carriers [17] which is not zero for $m = 1$ at the dark positions:

$$n(x) = n_0(1 + \tilde{m}\cos Kx), \qquad \tilde{m} < m. \tag{3}$$

The space-charge field is then given by Eq. (2) with m replaced by $\tilde{m}$. Poisson's law is applied to yield the corresponding charge density as

$$\rho(x) = \varepsilon\varepsilon_0\frac{\partial E_{\mathrm{sc}}(x)}{\partial x} = \tilde{m}\varepsilon\varepsilon_0\frac{k_BTK^2}{q}\,\frac{\tilde{m} + \cos Kx}{(1 + \tilde{m}\cos Kx)^2}. \tag{4}$$

A value for $\tilde{m}$ is calculated with this equation by requiring that at the completely dark grating positions ($m = 1$, $Kx = \pi$) the charge density ρ is limited by the trap density N_A in the crystal; i.e., we set $\rho_{(m=1,Kx=\pi)} = q(N_A + n)$. Since in $Bi_{12}SiO_{20}$, $n \ll N_A$ for the laser intensities used in the experiments [18], we neglect n. The additional assumption $\tilde{m} \sim m$ leads to

$$\tilde{m} = \frac{m}{1 + \varepsilon\varepsilon_0 k_BTK^2/q^2N_A}. \tag{5}$$

This approximation results in the same expression for the space-charge field E_{sc} as a linearized solution of the

Kukhtarev equations for small m [19]. For $m = 1$ the charge distribution calculated with Eq. (4) differs from the results of numerical solutions of the Kukhtarev equations [3] by less than 10%.

Equation (4) was used to fit the experimental data of Figs. 4 and 5. The theoretical results are shown as dotted lines in the figures. A value of 56 was used for $\varepsilon(Bi_{12}SiO_{20})$. The only parameter varied for the fit was the density of traps, N_A. All profiles in the two figures were calculated with the same value $N_A = 0.8 \times 10^{15}$ cm^{-3}. This compares favorably with the values found in the literature for different $Bi_{12}SiO_{20}$ crystals, which vary between 10^{15} cm^{-3} [20] and 10^{16} cm^{-3} [21].

As is obvious from the figures, this simple model almost perfectly reproduces the shape of the experimental profiles for different grating spacings in Fig. 4, and the shape as well as the amplitude of the charge gratings in Fig. 5. The only differences occur at larger fringe spacings where the width of the grating lines is slightly larger than for the theoretical curves. These discrepancies may be due to the fact that our simple model takes into account only one type of traps in the crystal (one-center model). It is well-known, however, that different types of traps occur in $Bi_{12}SiO_{20}$, among them shallow traps the density of which in some crystals may be as large as the density of deep traps [22].

Let us finally point out that the above calculation is one-dimensional; i.e., it refers to a crystal with infinite extension. When comparing the experimental results with this calculation, we therefore implicitly assume that the charge gratings are uniform up to the very surface. The range of the electrostatic force limits the depth for charge detection to about 10 nm. The properties of this outermost surface layer, however, may differ from the bulk, e.g., by adsorbed or diffused particles or by the effects of surface polishing.

In summary, we have demonstrated one possible application of charge detection with the AFM for the investigation of photorefractivity. The high-resolution mapping of charge gratings stored in photorefractive crystals allows us to study the profiles of such gratings obtained with different writing parameters. In the case of saturated gratings we successfully describe these profiles with a simple theoretical model. Such investigations will improve the understanding of the dynamics of the photorefractive effect. Further applications can make use of the combination of high sensitivity and high lateral resolution of the AFM measurements to investigate the nanostructure of the charge distribution which is related to crystal imperfections. This will be of practical importance for the development of photorefractive devices.

We thank Ch. Fabricius for theoretical assistance, V. I. Vlad for the crystal samples, and K. Buse for sharing his immense knowledge with us.

*Present address: Klugstrasse 49, 80638 München, Germany.

[1] K. Buse, Appl. Phys. B **64**, 273 (1997); **64**, 391 (1997).
[2] N. V. Kukhtarev, Sov. Tech. Phys. Lett. **2**, 438 (1976).
[3] A. Bledowski, J. Otten, and K. H. Ringhofer, Opt. Lett. **16**, 672 (1991).
[4] M. G. Moharam, T. K. Gaylord, and R. Magnusson, J. Appl. Phys. **50**, 5642 (1979).
[5] R. A. Rupp, Opt. Commun. **61**, 171 (1987).
[6] S. C. Som, S. K. Ghorai, and A. Satpathi, Opt. Quantum Electron. **25**, 241 (1993).
[7] S. Chiku, T. Horiuchi, T. Shiosaki, and K. Matsushige, Jpn. J. Appl. Phys. **34**, 5408 (1995).
[8] A. Shlensky *et al.,* Ferroelectrics **137**, 389 (1992).
[9] See, e.g., J. V. Alvarez-Bravo, M. Carrascosa, and L. Arizmendi, Opt. Commun. **103**, 22 (1993), and references therein.
[10] E. Soergel, W. Krieger, and V. Vlad, J. Opt. Soc. Am. B **15**, 2185 (1998).
[11] E. Soergel, W. Krieger, and V. Vlad, Appl. Phys. A **66**, S337 (1998).
[12] L. B. Schein, P. J. Cressman, and F. M. Tesche, J. Appl. Phys. **48**, 4844 (1977).
[13] B. D. Terris, J. E. Stern, D. Rugar, and H. J. Mamin, Phys. Rev. Lett. **63**, 2669 (1989).
[14] $Bi_{12}SiO_{20}$ crystal, transverse cut, nominally undoped, grown at the Institute for Atomic Physics, R-79600 Bucharest, Romania. The crystal surfaces were polished by the Crystal Laboratory of the Technical University, Munich, using colloidal silicia (Syton®, DuPont). The rms surface roughness value measured over an area of 10 μm $\times$ 10 μm is 0.2 nm.
[15] E. Soergel, Ph.D. thesis, University of Heidelberg, H. Utz Verlag GmbH, München, 1998.
[16] J. J. Amodei, Appl. Phys. Lett. **18**, 22 (1971).
[17] Ch. Fabricius (private communication).
[18] M. Peltier and F. Micheron, J. Appl. Phys. **48**, 3683 (1977).
[19] P. Yeh, *Introduction to Photorefractive Nonlinear Optics* (J. Wiley and Sons, Inc., New York, 1993), Chap. 3.
[20] J. P. Huignard, J. P. Herriau, G. Rivet, and P. Günter, Opt. Lett. **5**, 102 (1980).
[21] F. P. Strohkendl and R. W. Hellwarth, J. Appl. Phys. **62**, 2450 (1987).
[22] F. P. Strohkendl, J. Appl. Phys. **65**, 3773 (1989).